Available online at www.sciencedirect.com

ScienceDirect

Procedia Engineering 87 (2014) 827 – 830

Procedia Engineering

www.elsevier.com/locate/procedia

EUROSENSORS 2014, the XXVIII edition of the conference series

Investigation of the effects of hydrodynamic and parasitic electrostatic forces on the dynamics of a high aspect ratio MEMS accelerometer

F. Cerini[a,*], M. Ferrari[a], V. Ferrari[a], A. Russo[b], M. Azpeitia Urquia[b], R. Ardito[c], B. De Masi[c], A. Almasi[d], D. Iannuzzi[d], R. I.P. Sedmik[d]

[a]*Department of Information Engineering, University of Brescia, Italy*
[b]*STMicroelectronics, Italy*
[c]*Department of Civil and Environmental Engineering, Politecnico di Milano, Italy*
[d]*Department of Physics & Astronomy and LaserLaB, VU University Amsterdam, The Netherlands*

Abstract

We present the results of an extensive characterization of physical and electrostatic effects influencing the dynamical behavior of a micro-electromechanical (MEMS) accelerometer based on commercial technology. A similar device has been utilized recently to demonstrate the effect of Casimir and other nano-scale interactions on the pull-in distance [Ardito *et. al.*, Microelectron. Reliab., 52 (2012) 271]. In the present work, we focus on the influence of pressure, plate separation, and electric surface potentials on the spectral mechanical response. We finally find evidence for the presence of non-viscous damping due to compressibility of the ambient gas, and demonstrate a strong dependence of the sensitivity on the parameters of the operating point.

Peer-review under responsibility of the scientific committee of Eurosensors 2014

Keywords: MEMS accelerometer, dynamics, parasitic electrostatics, hydrodynamic damping, frequency shift

1. Introduction

Micro-electromechanical systems (MEMS) are employed in a wide variety of industrial applications. At the present technological level, typical surface separations in these devices are of the order of $1\,\mu$m. For these dimensions, it has already been demonstrated that hydrodynamic forces[1] and even Casimir [2, 3] interactions can influence the dynamical behavior of mechanical elements. The ongoing trend for miniaturization will necessitate the assessment and understanding of the prevalent interactions in the distance regime below the micrometer level. In this domain, due to the limitation of a maximum possible electric field strength, Casimir forces are necessarily of the same order as electrostatic ones. Therefore, one must either find ways to effectively reduce quantum-mechanical surface interactions [4], or to employ them in a controlled way to actuate devices [5]. Another aspect, which gains importance at small separations, is the presence of electrostatic 'patch' potentials caused by local variations in the Fermi surfaces. In the same way as Casimir forces, patch interactions create a pervasive force background which may cause stiction. Finally, even at low gas pressures, elastic hydrodynamic effects and slippage on surfaces have to be taken into account [6].

It is the purpose of the present work to investigate the aforementioned effects in a MEMS accelerometer based on commercial technology. We extend a previous characterization [3] of a similar device by an assessment of the influence of hydrodynamics and surface potentials onto the dynamic mechanical response.

*Corresponding author. phone: +39 030 3715938, email: fabrizio.cerini@ing.unibs.it

Peer-review under responsibility of the scientific committee of Eurosensors 2014
doi:10.1016/j.proeng.2014.11.279

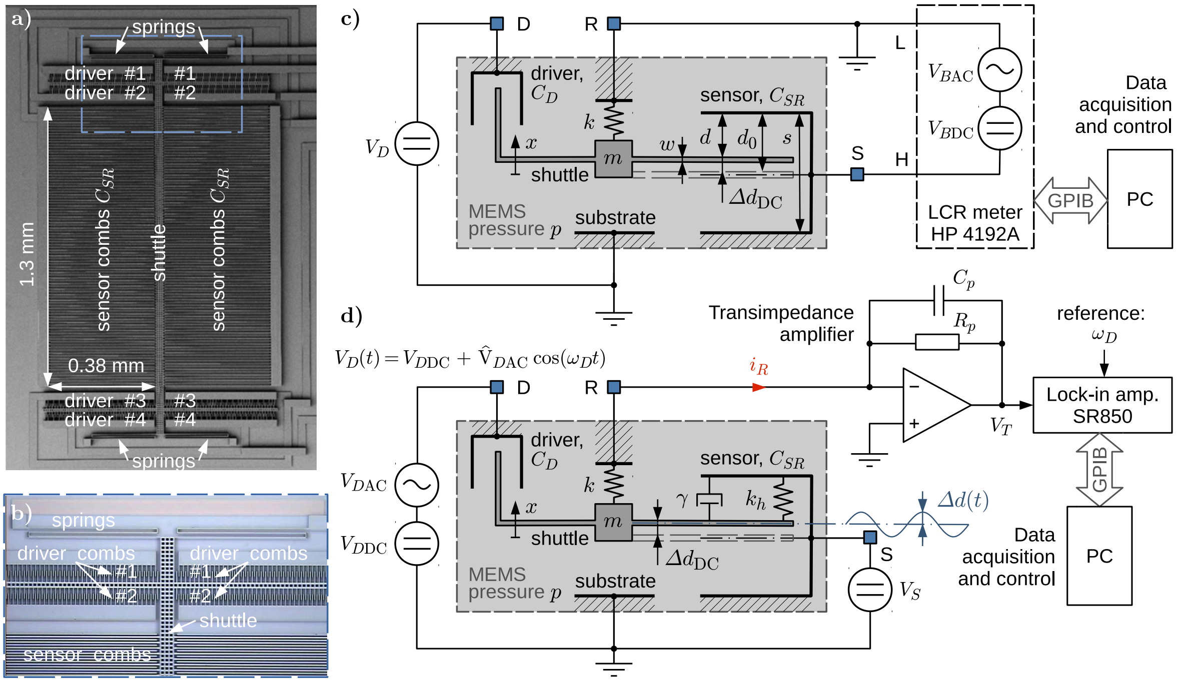

Fig. 1: Sensor and setup: a) SEM image of the entire accelerometer, where the frame indicates the area optically imaged in b). Schematic views of the setup for c) DC and d) AC measurements of the sensor response.

2. Device and setup

The investigated device has been designed and fabricated by ST Microelectronics using their *ThELMA* [7] process to create structures of 22 μm depth in heavily doped poly-silicon. As shown schematically in Fig. 1a, the mechanical structure consists of a movable shuttle (rotor, R) which is supported by four folded springs. Interleaved comb structures extending laterally from the shuttle form parallel plate capacitors with similar structures on the fixed frame (stator, S). Relative displacements [constant $\Delta d \equiv \Delta d_{\mathrm{DC}}$ and/or modulated $\Delta d \equiv \Delta d(t)$] between R and S, resulting in changes of the plate separation $d = d_0 - \Delta d$ can be sensed by monitoring the capacitance C_{SR},

$$C_{SR} = \varepsilon A \left(\frac{1}{d} + \frac{1}{s-w-d} \right) , \tag{1}$$

where A is the total sensing area, while s and w are the spacing between two S-lamellae and the width of an R-lamella, respectively. The device contains 4 linear bi-directional electrostatic comb drives (D), realized in two different geometries, one of which is shown enlarged in Fig. 1b). Application of a voltage V_D to D results in a force F_D on the shuttle in longitudinal direction x, and hence a displacement Δd according to,

$$\Delta d \approx \frac{F_D}{k} , \quad \text{with } k \equiv \lim_{\omega \to 0} T_{\Delta dF}^{-1} , \quad \text{where } T_{\Delta dF}^{-1} = m \left[\omega_r^2 - \omega^2 + 2 \mathrm{i} \xi \omega \omega_r \right] , \quad \text{and } d_0 = \lim_{F \to 0} d \, . \tag{2}$$

Here, m is the rotor mass, $\omega_r = 2\pi f_r = \sqrt{k/m}$ stands for the cyclic mechanical eigenfrequency, ξ is the viscous damping coefficient, and the elastic constant k represents the limiting value of the inverse mechanical transfer function $T_{\Delta dF}^{-1}$ relating general (driver and external) forces F to displacements Δd of the shuttle.
In order to measure the static and dynamic responses of the device, we utilize two different setups shown in Figs. 1c and 1d, respectively. Investigations of the pull-in distance and surface potentials are performed using a constant V_D to set Δd_{DC}, and an LCR meter with optional DC bias V_{BDC} applied between R and S. For dynamic measurements the system is excited by adding a modulation V_{DAC} at frequency $\omega_D/2\pi$ to V_D effecting a small vibration amplitude $\Delta d(t) \ll d$. This modulation together with the constant supply V_S results in a current $i_R = V_S \partial C_{SR}/\partial t$, which can be converted to a voltage via a transimpedence amplifier. Finally, demodulation by a lock-in amplifier synchronized to ω_D gives a signal which is proportional to $\Delta d(t)$. For the investigation of hydrodynamic effects, the setup is placed in a vacuum chamber allowing to control the pressure p_a.

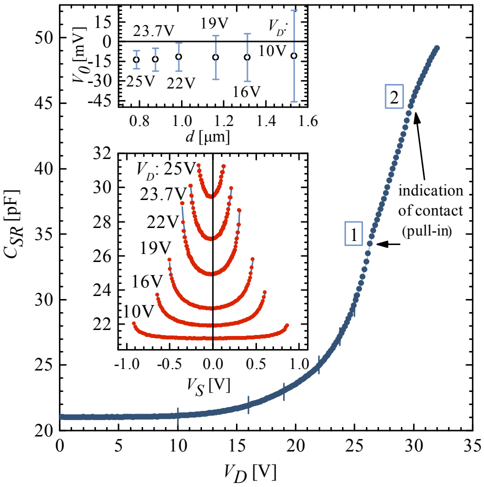

Fig. 2: Capacitance change versus applied driving voltage V_D (which alters d), as obtained in static measurements with the setup in Fig. 1c. Lower Inset: Change of C_{SR} at fixed positions d (set via Δd_{DC} by V_D) in dependence on the voltage V_S. The parasitic surface potential V_0 can be obtained from fits of the measured $C_{SR}(V_S)$ to Eqn. (1) with $\Delta d \propto (V_S - V_0)^2$, resulting in the data shown in the upper inset.

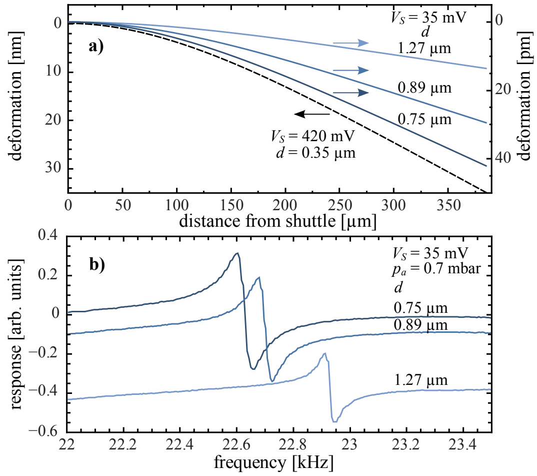

Fig. 3: Effects of lamellæ deformation. a) Numerical results for the deflection of R-lamellæ under the influence of V_S for various initial settings of d (solid curves, left scale pm). Assumed device tolerances may result for some lamellæ in a reduction of $d = 0.75 \rightarrow 0.35\,\mu$m, where the maximum applicable V_S above which pull-in of the lamella occurs is 420 mV (dashed line, left scale nm), which is to be compared to the values of $V_0 + V_S$ in Fig. 2. b) Electrostatic softening of the lamellæ at the same d and V_S (setup Fig. 1d).

3. Characterization of the device

Analytic modeling of driver characteristics is hampered by the strong influence of fringe effects [3, 8]. For this reason we resort to the simple model $F_D = f_D V_D^2$ and determine the geometrical factor f_D from a fit to DC measurements of C_{SR} shown in Fig. 2. The effective global V_0 can be determined either dynamically [10] or from the minima of the curves $C_{SR}(V_{B\mathrm{DC}})$ shown in the inset of Fig. 2). A minimization of the pull-in distance d_{pi} is possible by the application of a compensating voltage $V_{B\mathrm{DC}} = -V_0$. At small surface separations, non-linear effects become visible. These are caused by distance-dependent forces $F(d)$ (mainly electrostatic due to V_{BAC} and parasitic surface potentials V_0) and change the dynamics according to $k \rightarrow k_{eff} = k - \partial F(d)/\partial d$ and Eqn. (2), finally leading to instability and the infamous pull-in. However, apart from these well known effects, our device is also plagued by the softness of the lamellæ at small d. The latter deform under the influence of surface potentials V_S as shown in Fig. 3a, which leads to premature pull-in and further non-linear effects at $d \lesssim 0.8\,\mu$m. In this domain, force gradients lead to a reduction of the lamella resonance frequency f_{0L} [9] seen in Fig. 3b. Fabrication tolerances may explain the occurrence of multiple pull-in points observed in Fig. 2, at which supposedly (groups of) lamellæ snap to contact, thereby increasing k_{eff}.

The dynamical response of the mechanics depends on the precise parameters at the operating point. For sufficiently low damping ξ at pressures $p_a \lesssim 100\,\mu$bar, the amplitude reaches the bi-stability threshold as shown in Figs. 4a and b – an effect being strongly influenced by the modulation amplitude V_{DAC}. We determine the resonance frequency f_0 either from measurements of the oscillation [11] seen in step responses in Fig. 6, or from the minimum of the phase measured by the lock-in amplifier. While both measurements yield identical results (as demonstrated in Figs. 5a, c, and d), we believe that this method may be prone to uncertainties due to parasitic effects in the device requiring

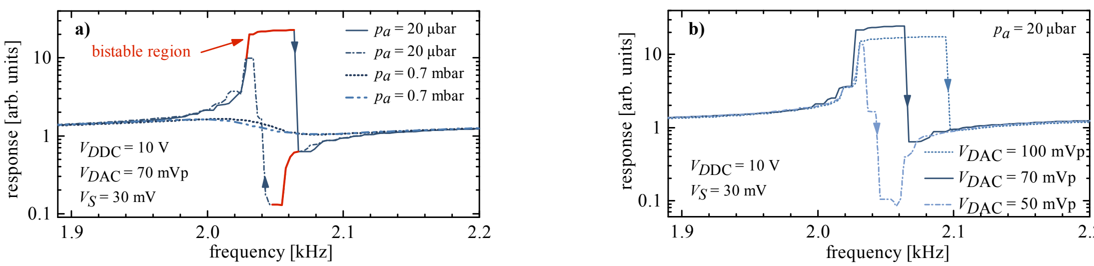

Fig. 4: Mechanical response at large distance ($d = 1.55\,\mu$m) obtained with the setup in Fig. 1d. a) Variation with the pressure p_a. Below $p_a \approx 100\,\mu$bar the amplitude increases sufficiently to trigger a nonlinear (bi-stable) response. b) The width of the bi-stability region depends on the oscillation amplitude given by the driver via V_{DAC}.

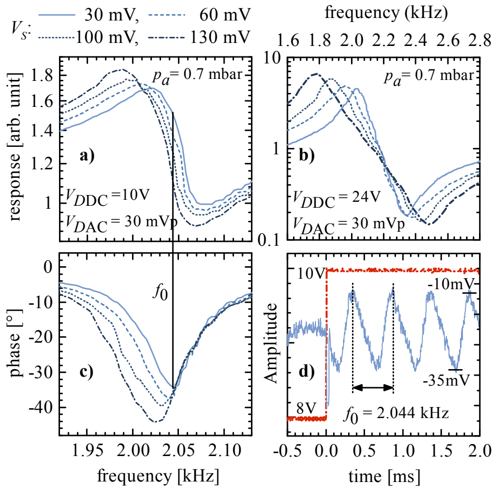

Fig. 5: Dynamic resposes (setup in Fig. 1d) at a) V_{DDC} = 10 V, d = 1.55 μm, and b) V_{DDC} = 24 V, d = 0.83 μm for various settings of V_S. While at large d an increase in the electrostatic force leads to a reduction in k_{eff} and the sensor resonance frequency f_0, the effect is eliminated at smaller distance, where to $\sigma > 10$ and elastic hydrodynamic effects compensate the effect of force gradients on k_{eff}. Measurements of f_0 from c) the phase minimum and d) the step response yield equal results.

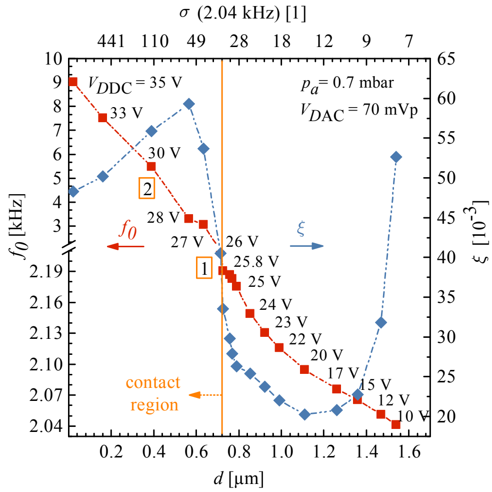

Fig. 6: Change of the mechanical response in dependence on the distance d. At large d, $\sigma \lesssim 10$ and the damping is mainly viscous [12], resulting in an unaltered f_0 and large ξ. When d is reduced, the elastic damping k_h increases with the gradually changing σ while the viscous component drops. Contrary, below $d \approx 1\,\mu$m, σ increases sharply, reasoning strongly augmented amplitudes of both ξ and f_0 until the first pull-in point (c.f. Fig. 2). The continued increase of ξ until the second pull-in may indicate that not all lamellæ are in contact.

additional modeling [11]. For this reason f_r and f_0 may differ. On the basis of preliminary model calculations, however, we consider the results in Fig. 6 to be qualitatively correct. It has been predicted (review: [6]) and measured [1] that at high squeeze numbers $\sigma = 12\eta\omega\ell^2/(p_a d^2) \gtrsim 10$, with the dynamic viscosity η of the ambient gas and ℓ being a typical device size for which we choose the depth of the lamellæ, the prevalent nature of fluid-interactions changes from viscous to elastic. Thereby, the softening effect of distance-dependent forces is countered according to $k_{eff} \rightarrow k - \partial F(d)/\partial d + k_h$. The coefficient k_h can be estimated from linearized Reynolds theory [12]. We find indications for such an increased k at small d ($\sigma > 10$) close to the pull-in, which are reflected by an increase in the measured resonance frequency seen in Fig. 6. More dedicated measurements could be performed using a MEMS-design with stiffer lamellæ, which would allow us to reduce d below 300 nm, thereby mimicking the hypothetical situation in future NEMS devices.

[1] M. Andrews, I. Harris, G. Turner, A comparison of squeeze-film theory with measurements on a microstructure, Sens. Act. A 36 (1) (1993) 79 – 87. doi:10.1016/0924-4247(93)80144-6.
[2] J. Zou, Z. Marcet, A. W. Rodriguez, M. T. H. Reid, A. P. McCauley, I. I. Kravchenko, T. Lu, Y. Bao, S. G. Johnson, H. B. Chan, Casimir forces on a silicon micromechanical chip, Nature Comm. 4 (2013) 1845. doi:10.1038/ncomms2842.
[3] R. Ardito, A. Frangi, A. Corigliano, B. D. Masi, G. Cazzaniga, The effect of nano-scale interaction forces on the premature pull-in of real-life micro-electro-mechanical systems, Microel. Reliab. 52 (1) (2012) 271 – 281, 2011 Reliability of Compound Semiconductors (ROCS) Workshop. doi:10.1016/j.microrel.2011.08.021.
[4] F. Intravaia, S. Koev, I. W. Jung, A. A. Talin, P. S. D. ad Ricardo S. Decca, V. A. Aksyuk, D. A. R. Dalvit, D. López, Strong Casimir force reduction through metallic surface nanostructuring, Nat. Commun. 4 (2515). doi:10.1038/ncomms3515.
[5] H. B. Chan, V. A. Aksyuk, R. N. Kleiman, D. J. Bishop, F. Capasso, Quantum Mechanical Actuation of Microelectromechanical System by the Casimir Force, Science 291 (2001) 1941. 10.1126/science.1057984.
[6] R. Pratap, S. Mohite, A. K. Pandey, Squeeze film effects in MEMS devices, J. Indian Inst. Sci. 87 (1) (2007) 75.
[7] A. Corigliano, B. De Masi, A. Frangi, C. Comi, A. Villa, M. Marchi, Mechanical characterization of polysilicon through on-chip tensile tests, J. Microelectromech. Sys. 13 (2) (2004) 200. doi:10.1109/JMEMS.2003.823221.
[8] H. Hammer, Analytical model for comb-capacitance fringe fields, J. Microelectromech Sys. 19 (1) (2010) 175. doi:10.1109/JMEMS.2009.2037833.
[9] C. Comi, A. Corigliano, A. Ghisi, S. Zerbini, A resonant micro accelerometer based on electrostatic stiffness variation, Meccanica 48 (8) (2013) 1893. doi:10.1007/s11012-013-9768-x.
[10] S. de Man, K. Heeck, D. Iannuzzi, No anomalous scaling in electrostatic calibrations for Casimir force measurements, Phys. Rev. A 79 (2) (2009) 024102. doi:10.1103/PhysRevA.79.024102.
[11] C. Comi, A. Corigliano, G. Langfelder, A. Longoni, A. Tocchio, B. Simoni, A resonant microaccelerometer with high sensitivity operating in an oscillating circuit, J. Microelectromech. Sys. 19 (5) (2010) 1140. doi:10.1109/JMEMS.2010.2067437.
[12] M. Bao, H. Yang, Squeeze film air damping in MEMS, Sens. Act. A 136 (1) (2007) 3, 25th Anniversary of Sensors and Actuators A: Physical. doi:10.1016/j.sna.2007.01.008.